Journal of Fusion Energy (2023) 42:43
https://doi.org/10.1007/s10894-023-00383-7

RESEARCH

In-operando Lithium Evaporation Inducing Helium Retention in Long-Pulse HIDRA Helium Plasmas

Andrew Shone[1] · Rabel Rizkallah[1] · Daniel O'Dea[1] · Brandon Kamiyama[1] · Daniel Andruczyk[1]

Accepted: 18 August 2023

Abstract

The Lithium Evaporation EXperiment (LEEX) campaign on the Hybrid Illinois Device for Research and Applications (HIDRA) investigates helium retention effects induced by *in-operando* lithium evaporations into HIDRA. Lithium droplets were applied to tungsten samples and then exposed to a 600 s helium plasma at different distances, D, from the plasma edge. LEEX data has confirmed previous results at the University of Illinois Urbana-Champaign of *in-operando* lithium evaporations producing a low recycling regime for HIDRA helium plasmas and additionally proves the retained species is helium. The lithium evaporation from the D = 25 mm case had an 85.3% ± 1% increase in helium retention in the low recycling regime when compared to the steady state plasma of the LEEX control shot. Data presented substantiates previous helium retention claims and advances research surrounding liquid metal PFCs. A retention mechanism has not been identified, but further research utilizing HIDRA aims to investigate this. This study's outcomes are thoroughly presented and provides additional justification for conducting further research on lithium's behavior in fusion environments, given its substantial potential impact on the development of PFCs.

Keywords Lithium · Helium retention · Liquid metals · Plasma-facing components · Plasma-material interactions

Introduction

The study of plasma-material interactions (PMI) is of paramount importance for the advancement of the field of fusion energy. Developing materials that can endure prolonged exposure to extreme conditions within a fusion reactor is crucial for rendering fusion energy a viable and economic alternative to current energy sources. A main research area of PMI encompasses the analysis of the interactions between the plasma and the wall of the fusion device, as well as the characterization of plasma behavior regarding wall interactions sending particles into the plasma [1–3]. Through precise manipulation of magnetic fields, the thermal load and particle flux of the plasma can be directed onto a specific region of the wall known as a divertor. The divertor is a critical plasma-facing component (PFC) and has traditionally been made from solid materials such as tungsten and molybdenum [4–6]. There have been several issues found with these high-Z divertor materials such as neutron damage causing embrittlement [7], tungsten fuzz formation [8, 9], and fuel retention [10]. To address and overcome the issues found with solid materials, researchers are exploring the use of liquid metals in divertor concepts.

Liquid-metal PFCs have a number of advantages over solid PFCs and, in recent years, lithium has emerged as one of the leading liquid metals for PFC development. Lithium is a low-Z material, has a low melting point (180.5 °C), and experimental thermoelectric magnetohydrodynamic systems have demonstrated controlled liquid lithium flows [11]. Liquid metals possess self-healing properties that can mitigate permanent damage caused by transient events such as edge-localized modes (ELMs) [12]. This assists in avoiding material degradation during the PFC's lifetime. Furthermore, studies have demonstrated that introducing lithium into the plasma, either intentionally or through PMI, can improve plasma performance [13–17]. The high chemical reactivity of lithium impedes impurity recycling from the walls, thereby enhancing plasma performance. Majeski et al. observed increased plasma performance via a low recycling regime in CDX-U when lithium was introduced [16].

✉ Andrew Shone
shone2@illinois.edu

[1] Center for Plasma Material Interactions, University of Illinois Urbana-Champaign, Urbana, IL, USA

Published online: 30 August 2023

The unique properties of lithium make it a compelling candidate for PFC development, as it has the potential to enhance plasma performance and reduce material degradation.

Lithium inducing a low recycling operating regime is beneficial in the case of helium ash removal in fusion devices. When the high-energy alpha particle created from a DT reaction [$D + T \rightarrow n\,(14.1\,MeV) + He\,(3.5\,MeV)$] collides with other particles in the plasma, it transfers its energy before thermalizing. This thermalized alpha particle is referred to as helium ash and is responsible for a decrease in plasma performance [18, 19]. Helium ash build-up severely deteriorates plasma performance and can halt fusion reactions from taking place in the plasma. Currently, there is no established way to efficiently remove helium ash which poses a significant issue in fusion device design. Lithium continues to be incorporated into PFCs and continues to show promising and advantageous properties which may be applicable to the issue of helium ash.

Recent experiments at the University of Illinois Urbana-Champaign (UIUC) reported unexpected observations of low recycling regimes in helium stellarator plasmas induced by *in-operando* lithium evaporations [20]. Experiments were conducted in the Hybrid Illinois Device for Research and Applications (HIDRA) and lithium evaporations were done utilizing the HIDRA-Material Analysis Test-stand (HIDRA-MAT) [21–23]. Typical helium plasma densities and temperatures in HIDRA are $n_e = 3 \times 10^{18}$ m^{-3} and $T_e =$ 20 eV, respectively. When lithium was evaporated into the helium plasma, neutral pressure decreased by an order of magnitude, helium spectral lines decreased despite constant electron cyclotron resonance heating (ECRH) and helium flow rate into HIDRA, and plasma density increased from $n_e = 3 \times 10^{18}$ m^{-3} to $n_e = 8 \times 10^{18}$ m^{-3}. While lithium was confined in the plasma, HIDRA operated in a low recycling regime, due to the reduction in background pressure, and plasma temperature increased from $T_e = 20$ eV to over T_e = 50 eV. Analysis of lithium and helium spectroscopic data and neutral pressure data yielded a correlation between a small amount of lithium ionization to the drop in helium lines and a decrease in neutral pressure. With a constant flow of helium gas into HIDRA, these data suggested background helium was actively being retained in HIDRA.

The helium retention behavior that was observed during two separate lithium evaporations into HIDRA helium plasmas are referred to as the Zeus shots [20]. Helium retention produced a low recycling regime that lasted for approximately 100 s during each 600 s pulse. Repeating the helium retention behavior asserted that this observation was an investigable phenomenon. The explanation of the Zeus shots used spectroscopy and pressure signals to connect lithium ionization to the measured helium reduction. Additional analysis of these data suggests there are chemistry effects responsible for the rapid decrease in impurities, such as reactions with oxygen and water, which can be explained by the high reactivity of lithium.

Building on the initial observations of helium retention in HIDRA, a secondary experimental campaign was launched named the Lithium Evaporation EXperiment (LEEX). The goal of LEEX was to reproduce what was seen in the Zeus shots and capture the necessary diagnostic data to prove helium retention was occurring. The Zeus shots provided preliminary data indicating the potential of helium retention, but LEEX aimed to gather more comprehensive data to demonstrate definitively that helium retention was occurring. This report will focus on experimental evidence showing lithium's involvement in helium retention in HIDRA and provide foundational support for future experiments to investigate the mechanism behind helium retention.

Experimental Setup

The objective of LEEX was to use a systematic approach to reproduce the results seen from the Zeus shots and collect additional data to verify previously observed helium retention in HIDRA was a real effect and not the result of an experimental oversight. Separate tests were conducted to examine the effect of the toroidal and helical magnets on the diagnostic operation and mass flow controller outputs. These tests yielded no indication that the magnets had any effect on the collection/output of these data from the diagnostics (excluding RGA data which is addressed in a subsequent section of this manuscript). The experimental procedure began by having a 99.95% tungsten sample baked out overnight at a temperature of ~200 °C. Post-bake out, the sample was heated to ~275 °C and then approximately 100 g of lithium was applied *in-vacuo* to the heated substrate using HIDRA-MAT's Liquid Metal Droplet Injector (LMDI) [24]. The heater provided a constant heat source to the sample once lithium was applied and throughout the plasma exposure. After lithium application, the sample was moved into position at a pre-determined distance, D, from the plasma edge. Four exposures were done as part of LEEX which included one exposure without lithium at D = 25 mm from the plasma edge, herein referred to as the control shot, and three exposures with lithium at three distances (D = 0 mm, 25 mm, and 47.5 mm). A new sample was utilized for every individual shot, but HIDRA was kept under vacuum between shots, so there was passivated lithium present on the walls from prior LEEX shots as the campaign progressed. Plasma shots are run before each LEEX evaporation to ensure plasma and diagnostic behavior are acceptable and exposure conditions are comparable between evaporations. The order of LEEX shots were the control shot, D = 0 mm, D = 47.5 mm, and

D = 25 mm. Analysis of the results showed no noteworthy effect on helium retention from having passivated lithium on the wall compared to a bare stainless steel wall. Each LEEX shot had a constant helium flow rate of 1 sccm throughout the 600 s exposure and a forward heating power of ~ 5 kW, mirroring the conditions of the Zeus shots. Post-exposure, the sample was retracted back into HIDRA-MAT for further characterization. Following surface characterization and cool-down of sample temperature and heater, HIDRA-MAT was brought up to atmosphere to substitute a new sample for the next evaporation shot.

HIDRA Upgrades

The experimental criteria for LEEX to be successful demanded that HIDRA and HIDRA-MAT were upgraded to have the ability to adequately test the hypothesis that helium retention was occurring during lithium evaporations. HIDRA was run as a stellarator because long-pulse plasmas were necessary to observe the transition from helium plasma to lithium plasma and, once the lithium was evaporated, the transition from lithium plasma back to helium plasma. The plasma shape was changed from an $\iota = 1/4$ to an $\iota = 1/3$ to prevent overlap between the plasma edge and ECRH antenna which had caused unwanted damage to the antenna in previous, high-power shots. An additional turbopump was installed to lower the base pressure of the main chamber to approximately 2×10^{-7} torr. This added pump increased pumping capabilities and reduced impurities inside of HIDRA resulting in a cleaner plasma operation.

A variety of diagnostics were added to HIDRA for LEEX and Fig. 1 shows the placement of each diagnostic on HIDRA. The final assembly of diagnostics on HIDRA included six PKR251 full-range pressure gauges, three SRS100 residual gas analyzers (RGAs), three cameras, two Ocean Insight spectrometers, MFC gas flow rate monitoring, and a reciprocating Langmuir probe (RLP). Spectroscopy data was collected using an HR2000 survey spectrometer with a usable spectral range of 350 – 1000 nm at 0.475 nm resolution. The full spectrum was measured every second with an integration time of 10 ms. The contribution of pressure gauge, RGA, and spectrometer data was pivotal in confirming the existence of helium retention, as they enable direct and independent measurements of helium. These diagnostics will be the focus of the results and discussion section.

HIDRA-MAT Upgrades

HIDRA-MAT has essential and unique capabilities which the LEEX campaign required. A rotatable sample head on an actuated linear transfer arm provided adjustment of the sample in HIDRA-MAT for sample preparation and characterization. Each sample in LEEX had a lithium drop applied to the heated sample (~ 275ºC) from the LMDI. After lithium application, the transfer arm enables quick movement and precise positioning of the sample in HIDRA for plasma exposure. The process of lithium application and sample movement was similar to the procedure followed in the Zeus shots with the main difference being the redesign of the sample head.

The Zeus Shots highlighted issues in HIDRA-MAT's design during lithium evaporations that were modified to produce better results in LEEX. Redesigning the sample

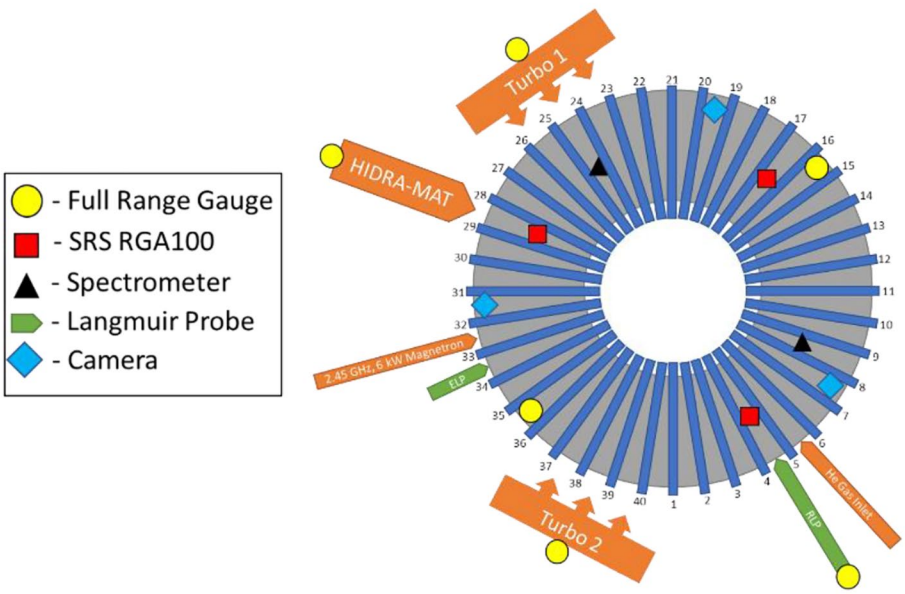

Fig. 1 A schematic top view of HIDRA showing LEEX's diagnostics. RGAs are positioned on the upper E-ports and spectrometers are positioned on the lower E-ports. Other diagnostics and pumps are connected to other HIDRA ports

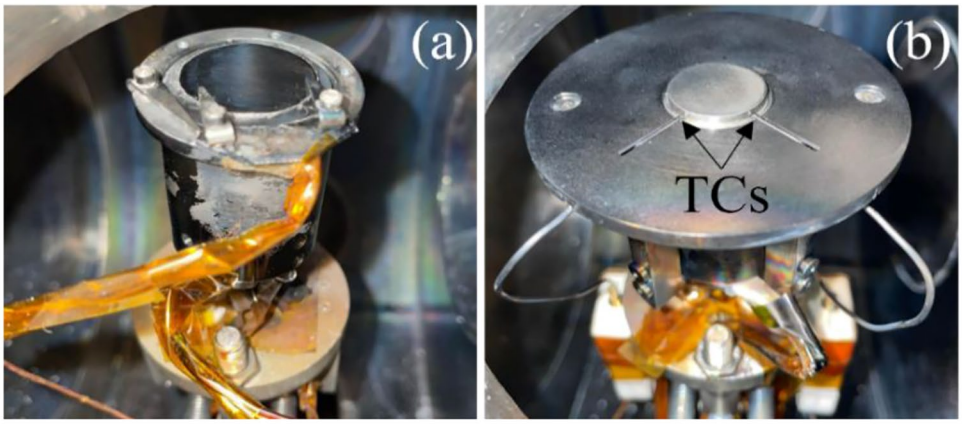

Fig. 2 The heater and sample holding configuration for the **(a)** Zeus shots and **(b)** LEEX campaign

head, seen in Fig. 2b, was the crucial step to establishing confidence towards consistent clean lithium evaporations and diagnostic measurements. The previous samples were cylindrical and were held on the UHV heater by molybdenum sample clips shown in Fig. 2a. This geometry forced the plasma to come into contact with the sample clips before the lithium. This interaction causes unwanted sheath formation at the clips and may have affected lithium evaporation dynamics. To overcome this issue, two changes were made. The sample was machined into a top hat formation, and a stainless steel sample cap was created to hold this sample on the heater. The sample cap holding the sample on the heater can be seen in Fig. 2b. Two slits for two thermocouples were added to the sample cap so temperature measurements could be collected and verified. In the Zeus shots, the thermocouples were exposed junctions that were replaced with sheathed ungrounded thermocouples to prevent the plasma from influencing data collection.

LEEX Results & Discussion

Spectroscopy Data

Two spectroscopic lines for helium (706 nm and 468 nm), and two spectroscopic lines for lithium (610 nm and 548 nm) correlate to an excited and ionized state, respectively, for both elements. These helium and lithium line intensities were analyzed throughout the exposure to understand the effect lithium evaporations had on the helium plasma. Data for each spectroscopic line of interest were compared across each LEEX plasma shot and are shown in Fig. 3. Figure 3a shows the helium 706 nm line for the control and D = 47.5 mm cases which exhibit the same behavior. When the ECRH system is turned on, there is a sharp rise, followed by a slow rise to a steady-state value after approximately 100 s into the shot. For the D = 47.5 mm case, the sample did not heat up enough to evaporate the lithium off the sample's surface, which was confirmed by two observations: inspection of the sample post-exposure showed the lithium droplet still on the sample surface, and the lithium signal in Fig. 3c and d is the same for the control and D = 47.5 mm case. The helium ion signal in Fig. 3b reaches a constant value for the control shot as soon as the plasma is struck while the D = 47.5 mm case shows a slight decrease in signal over the 600 s shot. There were no conclusions that could be made to explain the slight difference in trends. However, it can be concluded that having a liquid lithium droplet on a sample in the vacuum vessel, with little to no evaporation occurring, does not cause a measurable effect of helium pumping in HIDRA.

The trends observed in the D = 0 mm and D = 25 mm cases are in stark contrast to the other two cases because significant lithium evaporation occurred. Thermocouple data during the LEEX shots have suggested the sample temperature for significant lithium evaporation is close to 400 ^{o}C and both of these cases surpassed that temperature. Spectroscopy data in Fig. 3c and d show significant amounts of lithium being excited and ionized for these cases. Lithium evaporation happened sooner in the D = 0 mm case than the D = 25 mm case because heat flux to the sample was greater with the sample closer to the plasma edge. The timing of the increase and decrease of the 548 nm and 610 nm lithium lines match with each other for each case implying excitation and ionization happen in parallel. The increase in lithium in Fig. 3c and d correlates to the decrease in helium signal in Fig. 3a. As lithium evaporates into the plasma, the helium signal decreases until the lithium is depleted from the sample. Helium signal stays low as the evaporated lithium is confined in the plasma and then the helium signal begins to gradually rise as lithium is lost from the plasma to the walls. By the end of the shot in the D = 25 mm case, the helium signal had recovered to a steady-state value similar to the control shot.

There are unique features in Fig. 3a-d that provide valuable insight into the potential mechanisms of the observed

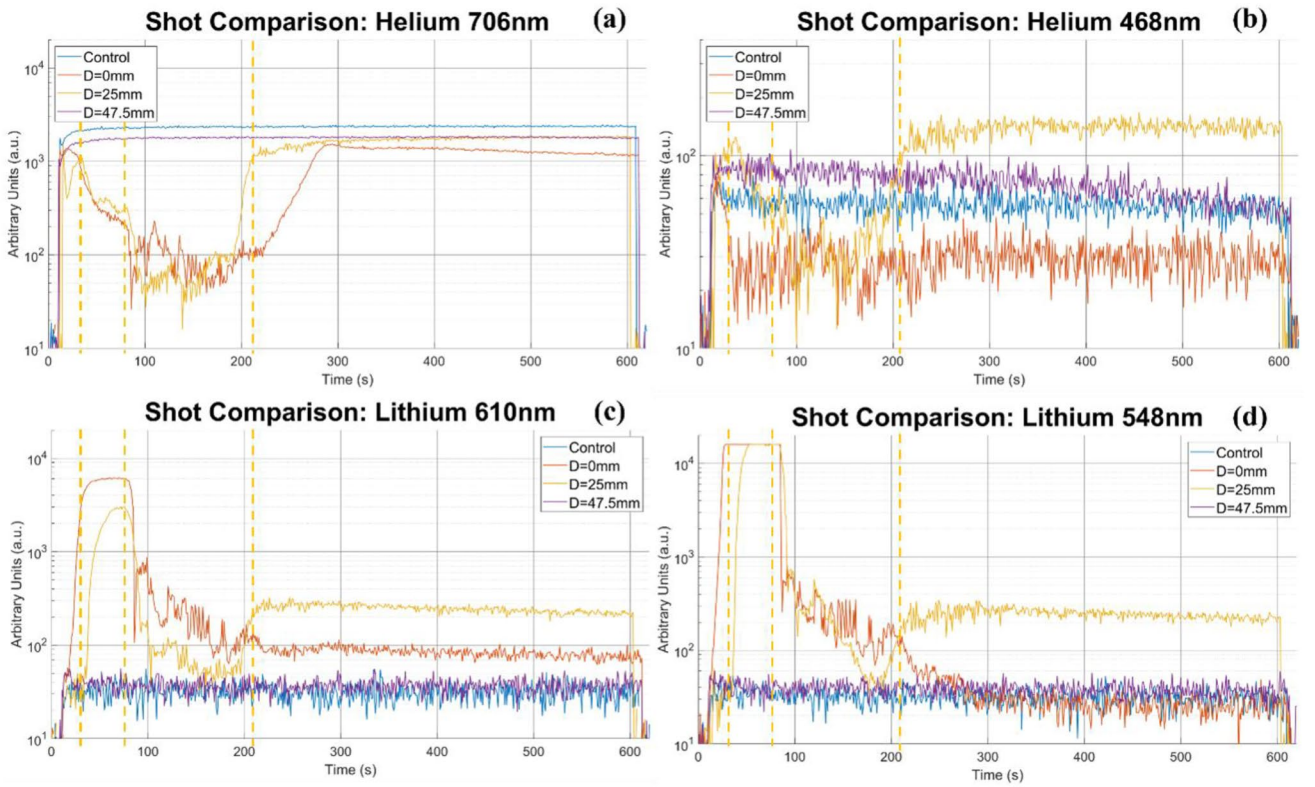

Fig. 3 Spectroscopy line data for each LEEX plasma compared to one another for **(a)** helium 706 nm, **(b)** helium 468 nm, **(c)** lithium 610 nm, and **(d)** lithium 548 nm lines. While helium reduction is linked to lithium excitation and ionization once lithium begins to evaporate into the plasma, the helium signal takes over 100 s to recover after the peak of these processes. For the D = 25 mm case, the first dashed line at t = 35 s shows an increase in lithium correlates to a drop in helium denoting the transition to the low recycling regime. The second dashed line at t = 76 s signals the peak of the lithium signal; however, the low recycling regime remains until the third dashed line at t = 215 s denoting when helium line intensity recovers

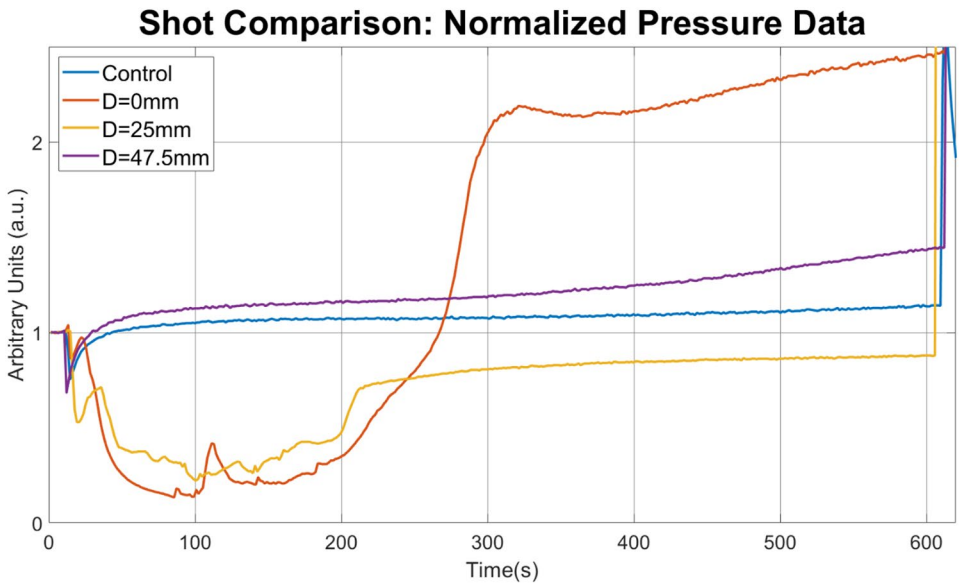

Fig. 4 Normalized pressure data for each LEEX plasma compared to one another. Cases where lithium evaporated from the W sample (D = 0 mm and D = 25 mm) had large decreases in pressure that lasted for > 180 s. These reduced pressure intervals are referred to as a low recycling regime

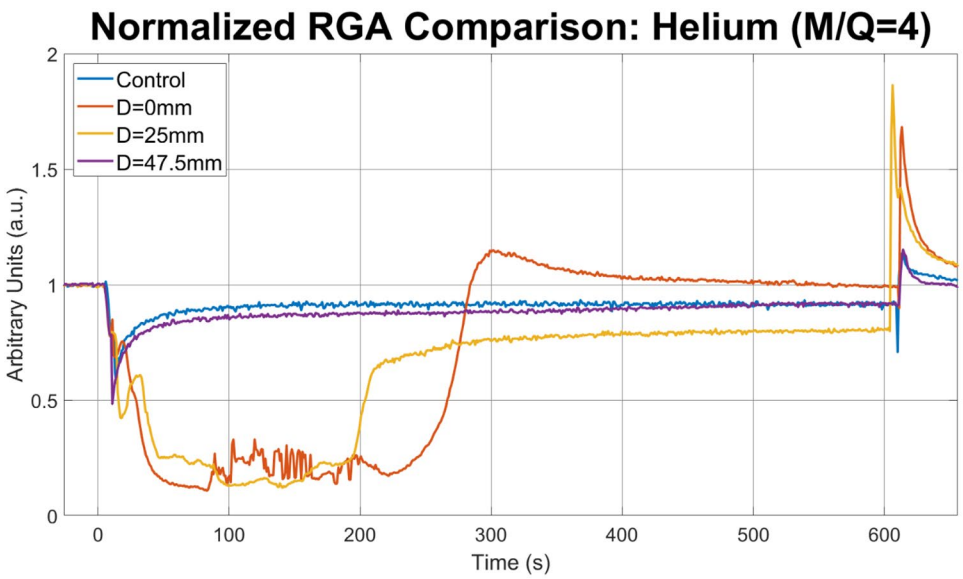

Fig. 5 Normalized RGA data for each LEEX plasma compared to one another. The data presented is taken from an RGA above the lithium evaporation position. Helium (M/Q = 4) RGA signal displayed decreases in the lithium evaporation cases proving the retained specie is helium in the low recycling regime

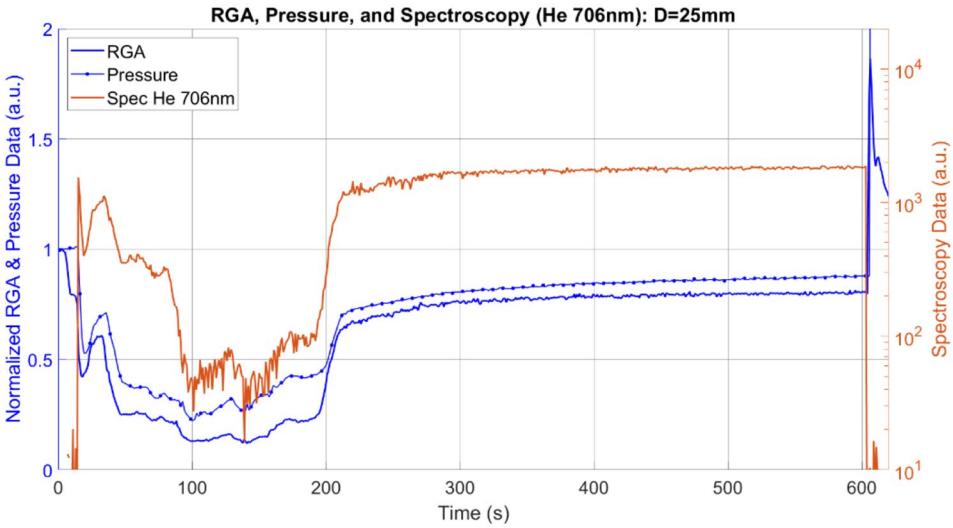

Fig. 6 Overlapping RGA, pressure, and spectroscopy (helium 706 nm) data shows the changes in signal for these three independent diagnostics correlate to one another. Matching trends from a variety of diagnostics gives confidence that the helium retention effect is real and not a diagnostic anomaly

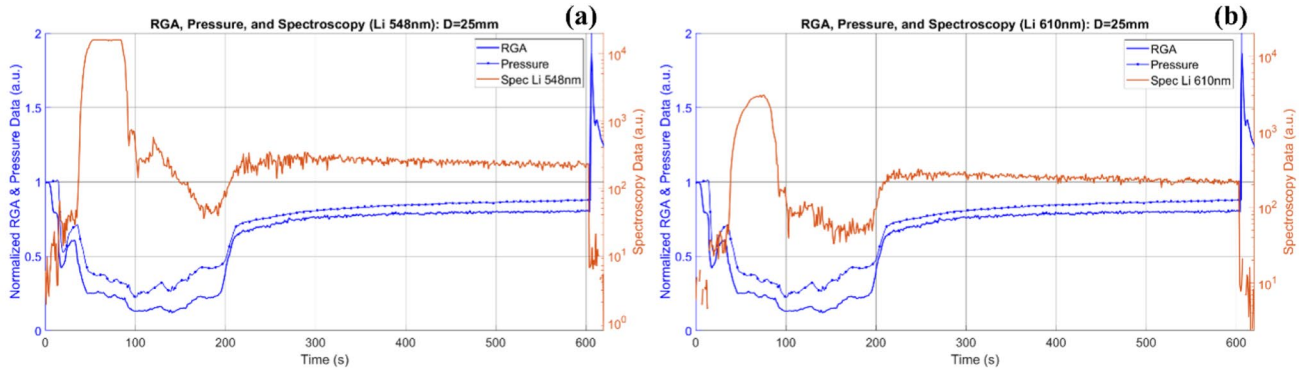

Fig. 7 Overlapping RGA, pressure, and spectroscopy data for two spectroscopy signals. Saturation of the (a) lithium 548 nm line indicates large amounts of ionization occurring once lithium evaporation occurs. The (b) lithium 610 nm signal is chosen in analysis because it does not saturate allowing for trends corresponding to the peak to be analyzed

helium retention effect. The first 35 s of the D = 25 mm case in Fig. 3a and c, and 3d, show a strong helium line intensity and low, but non-zero, lithium line intensity. At t = 35 s, there is a large increase in the lithium lines intensity, associated with significant lithium evaporation into the plasma, and the helium line intensity begins to decrease. This implies that there is a measurement threshold value to observe the retention effect. Comparing Fig. 3a, c and d, the rise in helium is not correlated to the large drop in lithium signal that happens at t = 76 s. Rather, the helium signal begins to rise > 100 s after the lithium intensity peak for both the D = 0 mm and D = 25 mm cases. The difference in the time it takes for the helium signal to rise may be attributed to the amount of lithium confined in the plasma. Although the amount of lithium evaporated for each case is the same, it can be assumed that more lithium makes its way into the core of the plasma for the D = 0 mm case. Therefore, it can be inferred that more lithium in the plasma would result in the retention behavior lasting longer. These data suggest that the measurement threshold for helium retention is extremely small, and the amount of lithium being evaporated into HIDRA during the shots is too much to accurately identify this threshold. Finally, the helium ion behavior in Fig. 3b for the D = 0 mm case is not directly associated with the trends seen in Fig. 3a as it is for the other cases. The ion signal falls with the initial decrease in helium, but never recovers and stays low. After the recovery of helium (i.e., after the helium signal rises close to pre-lithium evaporation levels), there is a slight increase in lithium signals for the D = 25 mm case, which may have contributed to the rise in ion signal. However, there is not enough information to explain this behavior.

Pressure Data

The main chamber pressure data for each shot was normalized to the constant pressure value before the shot and is presented in Fig. 4. Pressure data from all the full-range gauges on HIDRA followed the same trends as the one presented in Fig. 4 above. Figure 4 describes a similar trend to the spectroscopy data in Fig. 3a. When no lithium was evaporated into the plasma (control and D = 47.5 mm), the pressure initially decreases and then gradually rises. The control shot gradually rises until the ECRH is turned off. The D = 47.5 mm exhibits the same behavior but there is a larger increase in pressure during the shot. No discernable reason for this rise can be found in the current data other than a possible after-effect from the lithium evaporation (D = 0 mm) that took place before it. The D = 0 mm and D = 25 mm cases show a pressure increase at the beginning of the shot, presumably from PMI involving the lithium droplet. The pressure then decreases and increases in behavior similar to the other cases. However, once lithium begins to evaporate, a large pressure decrease is seen in D = 0 mm and D = 25 mm at t = 23 s and t = 35 s, respectively. These cases' pressure drop corresponds to the large influx of lithium being evaporated into the plasma shown by Fig. 3c and d.

Although the pressure trends in the lithium evaporation cases are similar, they are not identical. The D = 0 mm case shows a greater decrease in pressure but has more fluctuations during the low recycling regime due to increased PMI effects at the sample's edge. It is noteworthy that the pressure rise after the low recycling regime in the D = 0 mm case is much greater than the increase observed in any of the shots. This large increase in pressure may be attributed to enhanced PMI effects, caused by a hotter plasma ($T_e \geq 50$ eV), at the sample's surface once the lithium has been fully evaporated. In contrast, the D = 25 mm case shows a smaller decrease in pressure than the D = 0 mm case and experiences less PMI due to its position farther away from the plasma edge. Following the exhaustion of lithium, the pressure remains below the levels observed in the control shot to the end of the shot.

Residual Gas Analyzer Data

The addition of RGAs to the HIDRA main chamber provided another method of measuring helium content. Figure 5 shows the partial pressure of M/Q = 4 during the shot normalized to the constant values before the shot. For the purpose of this analysis, helium is assumed to contribute to the entirety of the M/Q = 4 signal since helium is the flowing gas. These data support both the spectroscopy data in Fig. 3a and the pressure data in Fig. 4 regarding helium retention behavior. Unlike spectroscopy and pressure data, the RGA is affected by HIDRA's helical magnetic field. The magnetic field is the cause of the initial drop in the RGA data during the t = 5–10 s interval during its ramp-up. Though there is an effect on the RGA, this same effect is present in every shot, thus the trends in the data can be compared. All three RGAs on HIDRA showed the same trends and Fig. 5 is taken from the RGA connected to the E-port above the sample location.

As in the previous datasets, the control and D = 47.5 mm cases exhibit a similar trend. In the D = 0 mm case, the drop in helium is observed, erratic signal is credited to PMI at the edge, and the rise in helium RGA signal follows the spectroscopy and pressure data. The decrease at 300 s can be matched with Fig. 3a and suggests the rise in pressure seen in Fig. 4 is not from an increase in helium. For the D = 25 mm case, two peaks in the first 50 s are present, one at t = 15 s and the other at t = 35 s, and the rest of the data coincides with spectroscopy and pressure data. The spikes at the end of each shot are from the ECRH system being

turned off and the magnets ramping down. RGA data can also be utilized to estimate the helium retention effect. The control shot steady-state value (taken as 100% recycling) is compared to the minimum values seen in the lithium evaporation cases to estimate retention for each shot. Using data measured in the D = 25 mm case, helium retention was calculated to be 85.3% ± 1% in the low recycling regime. This is a significant reduction in helium recycling and has never been observed in a toroidal device to the authors' knowledge.

Comparison of Spectroscopy, Pressure, and RGA Data

Figure 6 is the culmination of the spectroscopy, pressure, and RGA data for the D = 25 mm case discussed previously. This case is highlighted because the PMI between the sample assembly and plasma was reduced compared to the D = 0 mm case since the sample was farther from the plasma edge. Thus, there is more confidence that trends are from lithium-helium interactions for this case. Each dataset comes from an independent diagnostic that, when compared to one another, confirms the reduction of helium in HIDRA during a lithium evaporation is a real effect. Helium retention effects and a low recycling regime are present for ~ 180 s. Pressure shows a major reduction when compared to the control shot and the RGA and spectroscopy data confirm that the reduction of helium is occurring. Figure 7a and b show the relationship of ionized and excited lithium, respectively, to the reduction of helium seen in the pressure and RGA data. *In-operando* evaporation and subsequent excitation/ionization of lithium into the plasma introduces an influx of charged species as can be seen by the saturated lithium 548 nm ion signal and lithium 610 nm signal. However, the drop in helium signal begins before the peak in lithium signal suggesting that a small amount of lithium is needed for retention to occur. This statement is further supported when the large decrease in lithium signal observed between the t = 76–90 s interval does not induce as large of a change in the helium signal. The helium signal continues to decrease during this interval and then finds a relatively steady minimum value for ~ 100 s. It begins to rise again at t = 190 s and transitions out of the low recycling regime back to a standard helium plasma without lithium. There still are excited species and ionized species present in small quantities during the low recycling regime and that may be sufficient for elongating the retention effect.

Summary

The LEEX campaign at UIUC has confirmed that previously published data observing helium retention in HIDRA due to *in-operando* lithium evaporation [20] is a real and repeatable phenomenon. The helium retention phenomenon has now been reproduced four times in HIDRA and every instance of *in-operando* lithium evaporation in HIDRA resulted in helium retention. Upgrades to the sample geometry and the HIDRA-MAT sample holder improved the repeatability of shot conditions while limiting PMI which was detrimental to the durability of the previously used sample holder. Implementing more diagnostic capability through spectrometers, pressure gauges, and RGAs provided further insight into the effects these lithium evaporations have on helium plasmas in HIDRA. Spectroscopy, pressure, and RGA data show agreement in trends during each shot and add confidence that helium retention is occurring. Spectroscopic data from helium and lithium lines show a drop in helium signal coinciding with the rise in lithium signals. It is believed that only a small quantity of evaporated lithium is required to see the retention effect. A static droplet of lithium on the sample surface is not enough to generate the conditions needed for measurable retention. Spectroscopy and pressure data from LEEX mimic the data seen in the Zeus shots while the addition of the RGAs verify helium is the particle being retained by an unknown mechanism. The mechanism and the location at which the mechanism occurs, either at the wall or in the plasma, is still unknown. The leading hypothesis resulting from LEEX suggests helium retention is occurring at the walls of HIDRA. Helium atoms become trapped in voids and interstitial sites of a dynamically forming lithium lattice on the walls of the machine produced when lithium ions lose confinement from the plasma, stick to the wall, and cool down. An increase in helium line intensity would be measured spectroscopically during the low recycling regime if increased helium confinement was the cause of the measured RGA and pressure behavior. Since there is no evidence of this or any other spectral lines occurring that were not previously observed, retention at the wall is the most probable conclusion from the current data. Future experiments on HIDRA will aim to identify the helium retention mechanism, characterize the specific conditions required to produce retention in HIDRA, and elaborate on this hypothesis. Identifying the mechanism has the potential to have a monumental impact on PFC development. If an engineering solution that utilizes the retention mechanism can be integrated into current PFC designs, the issue of helium ash build-up in fusion devices could be mitigated.

Acknowledgements This work is supported by the Department of Energy DOE DE SC0017719, by the University of Illinois Urbana-Champaign Grainger College of Engineering, the Department of Nuclear, Plasma, and Radiological Engineering, the Office of the Vice Chancellor of Research, Facilities, Services at the University of Illinois at Urbana-Champaign. Special Thanks to the ongoing help and discussions from Max Planck Institute for Plasma Physics, Greifswald Germany.

Author Contributions Andrew Shone wrote the main manuscript text and prepared all the figures. Andrew Shone, Daniel Andruczyk, and Brandon Kamiyama conducted the experiments. All authors contributed to the analysis of experimental results. All authors reviewed the manuscript.

Declarations

Competing Interests The authors declare no competing interests.

This work was supported by the U.S. Department of Energy (Grant number DESC0017719).

The authors have no relevant financial or non-financial interests to disclose.

The authors have no competing interests to declare that are relevant to the content of this article.

All authors certify that they have no affiliations with or involvement in any organization or entity with any financial interest or non-financial interest in the subject matter or materials discussed in this manuscript.

The authors have no financial or proprietary interests in any material discussed in this article.

References

1. R. Parker, G. Janeschitz, H.D. Pacher, D. Post, S. Chiocchio, G. Federici, P. Ladd, J. Nucl. Mater. **241–243**, 1 (1997)
2. G. Federici, Phys. Scr. T. **T124**, 1 (2006)
3. G.F. Matthews, J. Nucl. Mater. **438**, S2 (2013)
4. A. Herrmann, H. Greuner, N. Jaksic, M. Balden, A. Kallenbach, K. Krieger, P. De Marné, V. Rohde, A. Scarabosio, G. Schall, Nucl. Fusion **55**, (2015)
5. G.F. Matthews, M. Beurskens, S. Brezinsek, M. Groth, E. Joffrin, A. Loving, M. Kear, M.L. Mayoral, R. Neu, P. Prior, V. Riccardo, F. Rimini, M. Rubel, G. Sips, E. Villedieu, P. De Vries, M.L. Watkins, Phys. Scr. T **T145**, (2011)
6. C.H. Wu, U. Mszanowski, J. Nucl. Mater. **218**, 293 (1995)
7. X. Hu, T. Koyanagi, M. Fukuda, Y. Katoh, L.L. Snead, B.D. Wirth, J. Nucl. Mater. **470**, 278 (2016)
8. M. Christenson, D. Panici, C. Moynihan, J. Wendeborn, J. Anderson, D.N. Ruzic, Nucl. Fusion **59**, (2019)
9. J.A.R. Wright, Tungsten. **4**, 184 (2022)
10. T. Loarer, C. Brosset, J. Bucalossi, P. Coad, G. Esser, J. Hogan, J. Likonen, M. Mayer, P. Morgan, V. Philipps, V. Rohde, J. Roth, M. Rubel, E. Tsitrone, A. Widdowson, Nucl. Fusion. **47**, 1112 (2007)
11. D.N. Ruzic, W. Xu, D. Andruczyk, M.A. Jaworski, Nucl. Fusion **51**, (2011)
12. H. Zohm, Plasma Phys. Control Fusion. **38**, 105 (1996)
13. D.K. Mansfield, K.W. Hill, and et, J.D. Strachan, Phys. Plasmas **1892**, (1996)
14. H.W. Kugel, M.G. Bell, J.W. Ahn, J.P. Allain, R. Bell, J. Boedo, C. Bush, D. Gates, T. Gray, S. Kaye, R. Kaita, B. Leblanc, R. Maingi, R. Majeski, D. Mansfield, J. Menard, D. Mueller, M. Ono, S. Paul, R. Raman, A.L. Roquemore, P.W. Ross, S. Sabbagh, H. Schneider, C.H. Skinner, V. Soukhanovskii, T. Stevenson, J. Timberlake, W.R. Wampler, L. Zakharov, Phys. Plasmas **15**, (2008)
15. G. Zuo, J. Hu, J. Li, N. Luo, L. Hu, J. Fu, K. Chen, A. Ti, L. Zhang, Plasma Sci. Technol. **12**, 646 (2010)
16. R. Majeski, R. Doerner, T. Gray, R. Kaita, R. Maingi, D. Mansfield, J. Spaleta, V. Soukhanovskii, J. Timberlake, L. Zakharov, Phys. Rev. Lett. **97**, 1 (2006)
17. A. Maan, E. Ostrowski, R. Kaita, D. Donovan, R. Majeski, D. Boyle, P. Hughes, E. Merino, T. Kozub, B.E. Koel, D. Elliott, T. Biewer, F. Scotti, V. Soukhanovskii, R. Lunsford, IEEE Trans. Plasma Sci. **48**, 1463 (2020)
18. D. Reiter, G.H. Wolf, H. Kever, Nucl. Fusion. **30**, 2141 (1990)
19. D. Reiter, H. Kever, G.H. Wolf, M. Baelmans, R. Behrisch, R. Schneider, Plasma Phys. Control Fusion. **33**, 1579 (1991)
20. D. Andruczyk, A. Shone, Z. Koyn, J.P. Allain, Plasma Phys. Control Fusion **64**, (2022)
21. R. Rizkallah, D. Andruczyk, A. Shone, D. Johnson, Z. Jeckell, S. Marcinko, Z. Song, D. Curreli, F. Bedoya, A. Kapat, J.P.P. Allain, M. Christenson, M. Szott, S. Stemmley, H. Sandefur, D.N.N. Ruzic, R. Maingi, J. Hu, G. Zuo, J. Schmitt, IEEE Trans. Plasma Sci. **46**, 2685 (2018)
22. R. Rizkallah, S. Marcinko, D. Curreli, M.S. Parsons, N. Bartlett, R. Gluck, A. Shone, D. Andruczyk, Phys. Plasmas **26**, (2019)
23. A. Shone, Z. Koyn, R. Rizkallah, D. O'Dea, A. Kapat, G. Golba, J. Hoffman, D. Kurukulasuriya, Q. Tang, A. de Castro, J.P. Allain, D. Andruczyk, J. Fusion Energy. **39**, 448 (2020)
24. A. Shone, Z. Koyn, B. Kamiyama, E. Perez, L. Barrus, N. Bartlett, J.P. Allain, D. Andruczyk, Fusion Eng. Des. **180**, 113193 (2022)